

January 2008

# A field-extrema hysteresis loss model for high-frequency ferrimagnetic materials

J. Cale

S. D. Sudhoff

R. R. Chan

Follow this and additional works at: <http://docs.lib.purdue.edu/ecepubs>

---

Cale, J.; Sudhoff, S. D.; and Chan, R. R., "A field-extrema hysteresis loss model for high-frequency ferrimagnetic materials" (2008).  
*Department of Electrical and Computer Engineering Faculty Publications*. Paper 31.  
<http://dx.doi.org/http://dx.doi.org/10.1109/TMAG.2008.921489>

This document has been made available through Purdue e-Pubs, a service of the Purdue University Libraries. Please contact [epubs@purdue.edu](mailto:epubs@purdue.edu) for additional information.

# A Field-Extrema Hysteresis Loss Model for High-Frequency Ferrimagnetic Materials

J. Cale, S. D. Sudhoff, and R. R. Chan

School of Electrical and Computer Engineering, Purdue University, West Lafayette, IN 47907-2035 USA

**We present a new field-extrema hysteresis loss model (FHM) for high-frequency ferrimagnetic materials, along with a parameter identification procedure. The model does not involve solving an ordinary differential equation (ODE) and is asymmetric in that it works well under dc bias conditions. In the proposed model, the loss calculations are based on the extrema values of the fields. The model includes the effects of magnetic saturation as well as frequency effects. The model is comparable in accuracy to the ODE-based Jiles–Atherton model, but retains the convenience and computational efficiency of an empirical model. We demonstrate a procedure to characterize the model parameters using the Jiles–Atherton model. We compare magnetic hysteresis loss calculated by our new model with a full time-domain solution, as well as an empirical model, for a sample high-frequency ferrite. We demonstrate the use of the model, and validate the model, by calculating magnetic loss in an EI core inductor operating as the filter inductor in a buck converter. The model and identification procedure are being endorsed as a useful framework for computing magnetic loss in the context of automated magnetic device design.**

*Index Terms*—Automated design, hysteresis, magnetic loss.

## I. INTRODUCTION

**A**UTOMATED, population-based design methods are becoming increasingly popular as design tools [1]–[6]. When using these algorithms (e.g., Monte Carlo, genetic algorithms, particle swarm optimization), it is common to require the analysis of  $10^4$ – $10^6$  individual designs. When performing such a procedure to minimize losses or maximize energy density, the fields within the device are different in each candidate design. Thus, a computationally efficient and accurate method of predicting magnetic losses is especially desirable in these cases.

Time-domain and history-dependent hysteresis models, in particular the well-known Jiles–Atherton and Preisach models, have been shown to accurately predict magnetic hysteresis losses and behavior. However, the computational time required by these models is inconvenient for automated design.

In an effort to mitigate the computational burden imposed by time and history-dependent hysteresis models, researchers have developed modifications to the empirical loss equation proposed by Steinmetz [7]–[11]. Since the Steinmetz equation is valid for sinusoidal excitations with zero dc bias, a particular goal of the research community was to extend the Steinmetz equation to predict loss attributable to nonsinusoidal flux density waveforms. Unfortunately, even these empirical models are not ideally suited for automated design algorithms.

One difficulty in applying [7]–[11] to automated design is that they require the time derivative waveform of flux density throughout the magnetic component. A high-resolution magnetic analysis over at least one period of the magnetization cycle is therefore needed.

The magnetic field solution for many useful magnetic devices is complicated by the device geometry, nonlinearity of the core material, and non-negligible leakage paths. A nonlinear finite-element analysis (FEA) is typically used to obtain the magnetic field solution for these devices. Furthermore, in many

cases a 3-D FEA is required to represent all leakage flux. However, because of the computational burden of FEA, it is not suitable in an automated design context. Even in the case where an accurate magnetic equivalent circuit that represents 3-D leakage paths is available, as in [12], obtaining the time derivative waveform of flux density still requires a high-resolution analysis.

A second difficulty in using these models relates to accuracy. Although empirical models based on the Steinmetz equation are a function of frequency, they rely on published Steinmetz parameters. In [7]–[11], these parameters are assumed to be constants. However, it is reported in [9], [11], and [16] that the Steinmetz parameters vary with frequency. For this reason, the accuracy of existing Steinmetz-based models is limited by the frequency range in which the underlying Steinmetz parameters are valid.

In this work, a novel hysteresis loss model and parameter identification procedure for high-frequency ferrimagnetic materials is demonstrated. The parameters from the model are obtained from a time-domain model (in this case the Jiles–Atherton model). In a sense, the proposed approach bridges the gap between empirical and time-domain models, in order to provide a suitable framework for automated magnetic device design.

The remainder of this paper is as follows. In Section II, the Jiles–Atherton and Steinmetz equation models are briefly reviewed. This is followed by a description of the proposed loss model in Section III. In Section IV, a characterization procedure is described for determining the parameters of the proposed loss model, and an example of obtaining the parameters of the proposed model from the Jiles–Atherton model for a sample high-frequency ferrimagnetic material is presented. The predicted power losses are also compared with an empirical model. In Section V, the proposed model is used to predict hysteresis loss in an EI core inductor, and this prediction is compared to that predicted using the Jiles–Atherton model and an empirical model. Power loss prediction using the proposed model will be shown to be in good agreement with the Jiles–Atherton model. The paper concludes with a summary and suggestions for future work.

## II. BACKGROUND

Two general approaches for computing magnetic losses are time-domain methods and empirical models. Among the common time-domain methods (notably the Jiles–Atherton and Preisach models), the Jiles–Atherton approach was chosen for this work.

Commonly used empirical models include: the original equation introduced by C.P. Steinmetz, herein referred to as the Classical Steinmetz Equation (CSE) [7], the Modified Steinmetz Equation (MSE) [8], the Natural Steinmetz Extension (NSE) [9], the Generalized Steinmetz Equation (GSE) [10], and the Improved Generalized Steinmetz Equation (iGSE) [11]. However, only the MSE contains terms that account for dc bias; the MSE will therefore be used to compare with the proposed model.

Descriptions of the Jiles–Atherton, CSE, and MSE are presented in the following subsections.

### A. Jiles–Atherton Hysteresis Model

A summary of the Jiles–Atherton model [13], [14] is given as follows:

$$\frac{dM_{\text{irr}}}{dH} = \frac{M_{\text{an}}(H_e) - M_{\text{irr}}}{k \operatorname{sig}\left(\frac{dH}{dt}\right) - \kappa[M_{\text{an}}(H_e) - M_{\text{irr}}]} \quad (1)$$

$$\frac{dM_{\text{rev}}}{dH} = c \left( \frac{dM_{\text{an}}}{dH} - \frac{dM_{\text{irr}}}{dH} \right) \quad (2)$$

$$M = M_{\text{irr}} + M_{\text{rev}} \quad (3)$$

$$M_{\text{an}} = M_s \left[ \coth\left(\frac{H_e}{a}\right) - \frac{a}{H_e} \right] \quad (4)$$

$$H_e = H + \kappa M \quad (5)$$

where  $M$  is the total magnetization,  $M_{\text{irr}}$  is the irreversible magnetization,  $M_{\text{rev}}$  is the reversible magnetization,  $M_{\text{an}}$  is the anhysteretic magnetization,  $H$  is the applied field,  $H_e$  is the effective field, and the parameters  $M_s$ ,  $k$ ,  $\kappa$ ,  $a$ , and  $c$  are parameters that describe the anhysteretic and quasi-static hysteresis loop. The function  $\operatorname{sig}(\cdot)$  is defined as  $\operatorname{sig}(x) = 1$  for  $x \geq 1$  and  $\operatorname{sig}(x) = -1$  for  $x < 1$ .

The model described by (1)–(5) can be put in an alternative form as

$$\frac{dM_{\text{irr}}}{dt} = \frac{M_{\text{an}}(H_e) - M_{\text{irr}}}{k \operatorname{sig}\left(\frac{dH}{dt}\right) - \kappa[M_{\text{an}}(H_e) - M_{\text{irr}}]} \frac{dH}{dt} \quad (6)$$

$$\frac{dM}{dt} = \frac{1-c}{1-c\alpha\frac{\partial M_{\text{an}}}{\partial H}} \frac{dM_{\text{irr}}}{dt} + \frac{c}{1-c\kappa\frac{\partial M_{\text{an}}}{\partial H}} \frac{dH}{dt} \quad (7)$$

where from (4)

$$\frac{\partial M_{\text{an}}}{\partial H} = \frac{M_s}{a} \left[ 1 - \coth^2\left(\frac{H_e}{a}\right) + \left(\frac{a}{H_e}\right)^2 \right]. \quad (8)$$

Solving (6)–(8) yields quasi-static magnetization loops. In [15], the Jiles–Atherton model was extended to include frequency effects. In particular, it was shown that in ferro- and ferrimagnetic materials, the frequency dependence of the coercivity is attributable to damped oscillation of the domain walls.

In particular, the frequency-dependent magnetization  $M_f$  is related to the quasi-static magnetization by

$$\frac{d^2 M_f}{dt^2} + 2\tau \frac{dM_f}{dt} + \omega_n^2 M_f = \omega_n^2 M \quad (9)$$

where  $\tau$  is a decay constant and  $\omega_n$  is the natural frequency of the magnetic moments (the frequency at which the moments would oscillate in the absence of damping forces). Once the quasi-static magnetization loops are obtained from (6)–(8), the frequency-dependent solution is determined from (9).

The complete frequency-dependent Jiles–Atherton model, as described by (6)–(9), will be used for time-domain simulations in the remainder of this section.

### B. Classical Steinmetz Hysteresis Loss Model

The CSE is a commonly used formula for approximating core losses of magnetic materials that are exposed to single-frequency, zero-bias excitation. According to the CSE, the hysteresis loss (per unit volume)  $P_{\text{CSE}}$  is simply

$$P_{\text{CSE}} = C f^\alpha B_{\text{max}}^\beta \quad (10)$$

where  $f$  is the frequency of the applied excitation,  $B_{\text{max}}$  is the maximum flux density in the material, and  $\alpha$ ,  $\beta$ , and  $C$  are empirical parameters which are assumed to be constant. The parameters in (10) are typically provided by manufacturers, either directly or in the form of loss curves.

### C. Modified Steinmetz Equation

The MSE is defined as follows. The average rate of induction (field intensity)  $\dot{B}_{\text{avg}}$  is defined as

$$\dot{B}_{\text{avg}} = \frac{1}{\Delta B} \int_0^T \left( \frac{dB}{dt} \right)^2 dt \quad (11)$$

where  $\Delta B = B_{\text{max}} - B_{\text{min}}$  is the change in induction over one cycle with time period  $T$ .

For sinusoidal excitation, the excitation frequency is related to the average rate of induction by

$$f = \frac{2}{\Delta B \pi^2} \dot{B}_{\text{avg}}. \quad (12)$$

An equivalent frequency  $f_{\text{eq}}$  is then defined for nonsinusoidal excitation as

$$f_{\text{eq}} = \frac{2}{\Delta B^2 \pi^2} \int_0^T \left( \frac{dB}{dt} \right)^2 dt. \quad (13)$$

The loss associated with each magnetization cycle is then

$$W_v = k f_{\text{eq}}^{\alpha-1} B_{\text{max}}^\beta. \quad (14)$$

The power loss for flux density waveforms (without dc bias) is then given as

$$P_{\text{MSE}} = (k f_{\text{eq}}^{\alpha-1} B_{\text{max}}^\beta) f \quad (15)$$

where  $f$  is the fundamental frequency.

In order to accommodate for dc bias, the following modification to  $k$  in (15) was suggested in [8]:

$$k_{\text{new}} = k_{\text{old}} \left( 1 - C_1 B_{\text{dc}} e^{-\frac{B_{\text{ac}}}{C_2}} \right) \quad (16)$$

where  $B_{\text{dc}}$  and  $B_{\text{ac}}$  are associated with the dc and ac portion of the flux density waveform and  $C_1, C_2$  are constants that are determined experimentally from measurements at different frequencies and magnetizations.

### III. DESCRIPTION OF THE PROPOSED MODEL

Although the CSE is simple in form, its application is limited. First, the model does not account for dc bias in the flux density. Secondly, although (10) is a function of frequency, it has been suggested that the CSE parameters themselves vary with frequency [16]. On the other hand, the MSE accounts for dc bias by the addition of (16). Even so, the MSE requires knowledge of the derivative of flux density over a time period for the calculation of  $f_{\text{eq}}$ .

In addition to these concerns, in many engineering applications that incorporate magnetic devices, the measured or controlled quantity is input current. For these applications, it is convenient to formulate the hysteresis loss model in terms of the minimum and maximum source field.

It is desired that the new model addresses the needs stated above while approaching the accuracy of a time-domain simulation without the associated computational time. To this end, the proposed field-extrema hysteresis model (FHM) has the form

$$P_{\text{FHM}} = \zeta(f)z(\Delta M_{\text{an}})w(\Delta H) \quad (17)$$

where

$$\zeta(f) = \sum_{j=1}^J s_j f^{m_j} \quad (18)$$

and  $z(\cdot)$  and  $w(\cdot)$  are functions such that  $z(0)=0$  and  $w(0)=0$ .

In this work

$$z(\Delta M_{\text{an}}) = \sum_{k=1}^K \gamma_k \left( \frac{\Delta M_{\text{an}}}{M_s} \right)^{b_k} \quad (19)$$

$$w(\Delta H) = \sum_{l=1}^L \rho_l (\Delta H)^{r_l} \quad (20)$$

where  $\Delta M_{\text{an}} = M_{\text{an}}(H_{\text{max}}) - M_{\text{an}}(H_{\text{min}})$  and  $\Delta H = H_{\text{max}} - H_{\text{min}}$ .

Without loss of generality, the leading coefficients in (19)–(20) may be chosen as  $\gamma_1 = 1, \rho_1 = 1$ .

As seen from (17), the FHM incorporates the dc bias by leaving  $H_{\text{min}}$  and  $H_{\text{max}}$  unspecified. In addition, the coefficients in the polynomial expansion in (18) determine the frequency effects of the model.

Although the proposed model is not ODE based, it is not without physical justification. For steady-state conditions, the hysteresis loss density may be expressed in terms of the area enclosed by the trajectory of  $B$  and  $H$  in the  $B$ – $H$  plane.

The height and width of the circumscribing rectangle are  $M_{ah}(H_{\text{max}}) - M_{ah}(H_{\text{min}})$  and  $H_{\text{max}} - H_{\text{min}}$ , respectively. This suggests the use of these terms as the basis for (17).

In general ferrites, the dissipative processes at low frequencies are different than at high frequencies. In particular, at low frequencies, annihilation, formation, and movement of domain walls dominate losses. At high frequencies, eddy currents dominate losses. The ability of the proposed approach to extrapolate from the static-hysteresis loop to predict higher frequency ac losses is to some extent due to the restriction of the application of the method to high-frequency ferrites which have high resistivity and thus low eddy-current losses.<sup>1</sup> The ability to extrapolate is also due to the fact that the Jiles–Atherton model used to parameterize the FHM includes the effects of loss mechanisms beyond the static hysteresis loop (for example, minor loop behavior).

### IV. CHARACTERIZATION OF MODEL PARAMETERS

In the first part of this section, the identification procedure for the parameters of the FHM is cast as an optimization problem. This is followed by characterizations of a sample ferrimagnetic material for zero bias and dc bias conditions.

Note that it is possible to determine a single set of parameters that will cover both zero bias and dc bias applications. However, utilizing separate characterizations allows the model parameters to be tailored to the two applications. This yields better performance and/or allows the use of fewer terms in (18)–(20).

#### A. Formulation of the Optimization Problem

The optimization problem of determining the coefficients in (18)–(20) will now be posed. To this end, define the parameter vector to be determined as

$$\boldsymbol{\theta} = [m_1 \dots m_J s_1 \dots s_J b_1 \dots b_K \dots \gamma_2 \dots \gamma_K r_1 \dots r_L \rho_2 \dots \rho_L]. \quad (21)$$

The next step is to generate  $N_s$  sample excitation waveforms and to collect the minimum and maximum field and frequency points. The magnetizations corresponding to the  $N_s$  sample excitation waveforms are then computed using the frequency-dependent Jiles–Atherton model described by (6)–(9).

The error  $E(\boldsymbol{\theta})$  associated with each set of parameters  $\boldsymbol{\theta}$  are then defined as

$$E(\boldsymbol{\theta}) = \frac{1}{N_s^{1/P}} \left( \sum_{n=1}^{N_s} \left| \frac{P_{\text{FHM},n} - P_{\text{JA},n}}{P_{\text{JA},n}} \right| \right)^{1/P} \quad (22)$$

where  $P_{\text{JA},n}$  is the power loss associated with the  $n$ th waveform computed from the Jiles–Atherton simulation and  $P_{\text{FHM},n}$  is the power loss as calculated using the proposed model with parameter vector  $\boldsymbol{\theta}$ .

The fitness for the parameter vector  $\boldsymbol{\theta}$  is defined as

$$f(\boldsymbol{\theta}) = \frac{1}{E(\boldsymbol{\theta}) + \varepsilon} \quad (23)$$

<sup>1</sup>These comments were suggested by one of the paper's reviewers. The authors appreciate this contribution.

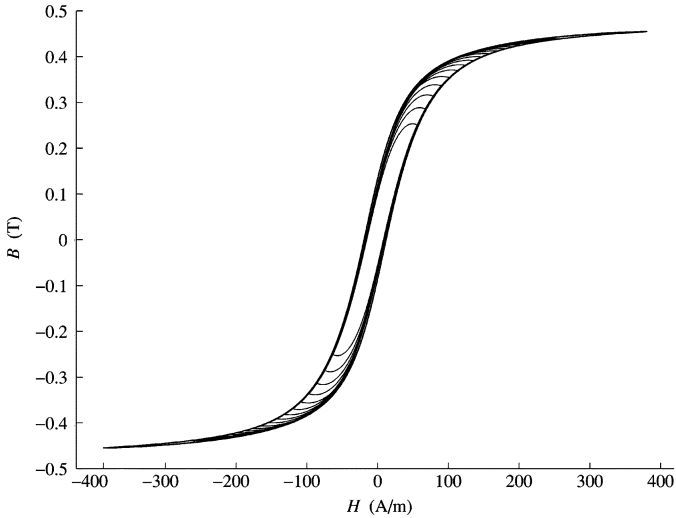


Fig. 1. Hysteresis loops obtained from Jiles–Atherton simulation: zero dc bias.

where  $\varepsilon$  is a small number ( $10^{-10}$ ) introduced to avoid a singularity in the unlikely event of a perfect fit.

Any optimization method can be used to maximize (23). In the case studies that follow, a genetic algorithm was used [17]–[19]. The genetic algorithm used was implemented in MATLAB 7.0 [21], [22] and was part of the GOSET toolbox [23].

The sample material was a FerroxCube 3C81 ferrite [20], having the hysteresis parameters  $M_s = 0.4 \cdot 10^6$  (A/m),  $k = 30$  (A/m),  $a = 27$  (A/m),  $\kappa = 5 \cdot 10^{-5}$ ,  $c = 0.55$ ,  $\tau = 10^{-6}$  (s), and  $w_n = 3.86 \cdot 10^6$  (rad/s) [15].

### B. Characterization of Parameters: Sinusoidal AC Case

In this example characterization, the parameters of the FHM were determined for the sinusoidal, zero dc bias case. Such characterizations are useful for line-frequency component designs.

First,  $N_s$  training field waveforms were defined as

$$H_n(t) = H_{f,n} \sin(2\pi f_n t). \quad (24)$$

Magnetic power loss was then computed for each of the waveforms using the Jiles–Atherton model. Several of the waveforms obtained from the Jiles–Atherton model are shown in Fig. 1.

Taking  $J = 2$ ,  $K = 1$ ,  $L = 1$ , and  $P = 2$  in (18)–(22), minimum and maximum values for the parameter values were selected to be

$$\theta_{mn} = \underbrace{[10^{-3} 10^{-4}]}_{m_j} \underbrace{[1 10^{-5}]}_{s_j} \underbrace{[10^{-2} 10^{-3}]}_{b_1 \quad r_1} \quad (25)$$

and

$$\theta_{mx} = \underbrace{[50 5 10^5]}_{m_j} \underbrace{[1 50]}_{s_j} \underbrace{[50]}_{b_1 \quad r_1}. \quad (26)$$

The total number of individuals in the population and number of generations were taken to be  $N_p = 2000$  and  $N_g = 1000$ . It was observed that convergence was obtained in 500 generations.

A plot of the Jiles–Atherton predicted losses (plotted with an “o”) and the FHM predicted losses (plotted with an “x”) using the parameters obtained using the proposed fitting process is

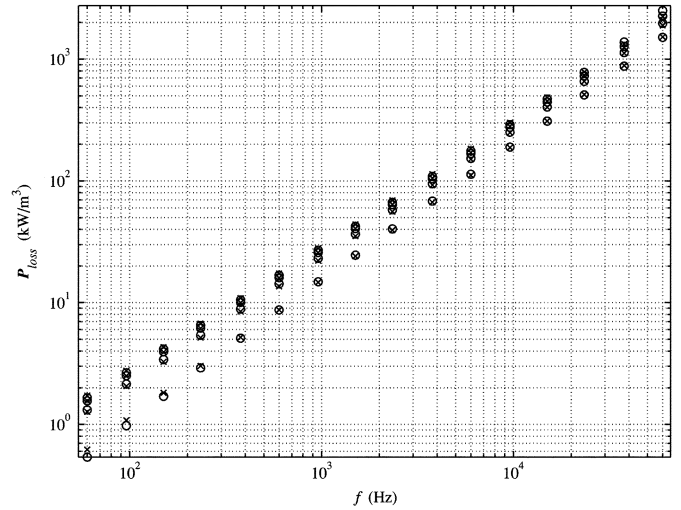


Fig. 2. Fit for FHM predicted loss (x) versus Jiles–Atherton predicted loss (o).

TABLE I  
PARAMETERS OBTAINED FOR  $P_{\text{FHM}}$ : ZERO DC BIAS CASE

Parameter	Value	Parameter	Value
$m_1$	$9.77 \cdot 10^{-1}$	$s_1$ (J/Wb·m)	6.44
$m_2$	1.18	$s_2$ (J/Wb·m)	$4.36 \cdot 10^{-1}$
$b_1$	1.69	$r_1$	$6.90 \cdot 10^{-2}$

shown in Fig. 2. Each pair of points (x and o) corresponds to a separate experiment. Different pairs of points at the same frequency have different excitation waveforms. As can be seen, the proposed model performed well in reproducing the loss predicted by the Jiles–Atherton model for the training data set. The average error for the samples was 3.3%. This yielded the parameters shown in Table I.

For zero dc bias sinusoidal waveforms, the MSE reduces to the CSE. Thus, in order to compare the power losses predicted by the FHM and the MSE, as well as to obtain the Steinmetz parameters required by the MSE in subsequent case studies, the parameters in (15) were determined. Since there were only three parameters in this case, minimization of the average error between the predicted losses from the MSE and Jiles–Atherton model was obtained from curve-fitting techniques (Nelder–Mead simplex [24]). The best fit parameters obtained were  $\alpha = 1.02$ ,  $\beta = 1.92$ , and  $C = 30.6$  (J/Wb · m).

Ten sample waveforms of the form of (24), but different from the training waveforms, were then generated. The magnetic power losses associated with the ten sample waveforms using the FHM and MSE (with their fitted parameters) were then compared with the losses obtained from the Jiles–Atherton model. Table II lists the sample waveform data and the power losses. As shown at the bottom of Table II, the losses obtained from both models were comparable to the Jiles–Atherton model in the zero dc bias case, although the FHM performed slightly better than the MSE.

In order to further validate the FHM, the performance was next tested for situations in which harmonic content is present. This could be due to magnetic saturation in a filter inductor or space-harmonics in an electromagnetic device.

TABLE II  
COMPARISON OF CALCULATED POWER LOSS FROM  
TIME-DOMAIN ANALYSIS VERSUS MSE AND FHM

$H_f$ (A/m)	$f$ (kHz)	$P_{JA}$ (kW/m <sup>3</sup> )	$P_{MSE}$ (kW/m <sup>3</sup> )	$P_{FHM}$ (kW/m <sup>3</sup> )
279.27	10	1635.6	1422.3	1506.7
80.82	20	603.2	600.3	619.6
53.36	30	399.1	437.6	464.4
142.43	40	439.2	435.9	440.0
224.66	50	1281.5	1174.4	1227.8
272.34	60	1031.1	964.9	1009.2
198.45	70	1523.8	1369.4	1434.1
89.18	80	778.3	757.9	783.7
129.17	90	174.6	175.2	173.7
108.35	100	204.3	204.5	203.5
		Avg. Error (%)	5.2	4.1

TABLE III  
COMPARISON OF CALCULATED POWER LOSS FROM  
TIME-DOMAIN ANALYSIS VERSUS MSE AND FHM

$H_f$ (A/m)	$f$ (kHz)	$P_{JA}$ (kW/m <sup>3</sup> )	$P_{MSE}$ (kW/m <sup>3</sup> )	$P_{FHM}$ (kW/m <sup>3</sup> )
279.27	10	1721.1	1502.3	1482.5
80.82	20	576.2	622.0	586.9
53.36	30	366.9	450.8	431.0
142.43	40	434.2	455.7	426.8
224.66	50	1324.6	1236.8	1204.1
272.34	60	1068.0	1019.2	992.6
198.45	70	1573.7	1439.3	1204.1
89.18	80	752.4	786.5	745.9
129.17	90	170.3	182.9	167.9
108.35	100	197.3	212.8	195.4
		Avg. Error (%)	8.8	6.5

First, power loss was computed using the Jiles–Atherton model with  $N_s$  input waveforms defined as

$$H_n(t) = H_{f,n} \sin(2\pi f_n t) + 0.3H_{f,n} \sin(6\pi f_n t - \pi/6) \quad (27)$$

where  $H_{f,n}$  are the same as those used in the zero dc bias characterization above.

The magnetic power losses associated with the waveforms in (27) were then computed using the FHM and MSE with the parameters obtained from the purely sinusoidal zero dc bias fit. Note that because of the third harmonic term  $H_{\max,n} = -H_{\min,n} \neq H_f$ , therefore  $H_{\max,n}$  must be calculated as the maximum of (27) when applying the FHM.

Table III lists the sample waveform data and the power losses. As shown at the bottom of Table III, the losses obtained from both models were comparable to the Jiles–Atherton model, although again the FHM performed better than the MSE. It is interesting to note that the FHM model is reasonably accurate even though (27) includes two minor loop traversals with the  $B$ – $H$  trajectory. A distinct advantage of the FHM in this application is that to utilize the FHM, only the peak fields need be calculated—it is not necessary to calculate the magnetization over a complete field cycle in order to compute the magnetic power loss.

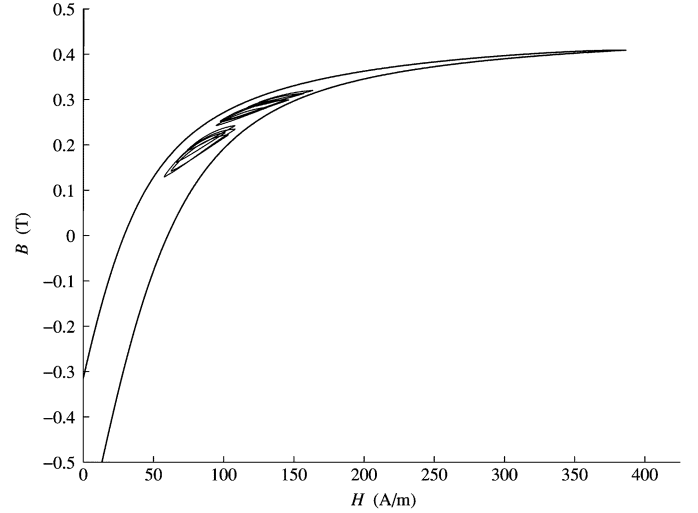


Fig. 3. Hysteresis loops obtained from Jiles–Atherton simulation: dc bias case.

### C. Characterization of Parameters: DC Bias Case

In this characterization, the parameters of the FHM for the dc bias case were obtained for triangular waveforms with dc bias. Such characterizations are useful for power electronic converter applications.

The  $N_s$  training field waveforms were defined as

$$H_n(t) = \begin{cases} \frac{\Delta H_n}{DT} t + H_{\min,n} & 0 \leq t \leq DT \\ -\frac{\Delta H_n}{(1-D)T} (t - DT) + H_{\max,n} & DT < t \leq T \end{cases} \quad (28)$$

where  $D$  and  $T$  are duty cycle and switching period, respectively, and  $\Delta H_n = H_{\max,n} - H_{\min,n}$ .

Magnetic power loss was then computed for each of the waveforms using the Jiles–Atherton model. Several of the waveforms obtained from the Jiles–Atherton model are shown in Fig. 3. Note that in this figure, the major loop shown is the quasi-static loop which is provided for context. It is not part of any of the trajectories.

Taking  $J = 2$ ,  $K = 1$ ,  $L = 1$ , and  $P = 2$  in (18)–(22), minimum and maximum values for the parameter values were selected to be

$$\theta_{\min} = \underbrace{[10^{-6} 10^{-6} 10^{-6} 10^{-6} 10^{-6} 10^{-6}]}_{m_j \quad s_j \quad b_1 \quad r_1} \quad (29)$$

and

$$\theta_{\max} = \underbrace{[10 \ 10 \ 10 \ 10 \ 10]}_{m_j \quad s_j \quad b_1 \quad r_1}. \quad (30)$$

The total number of individuals in the population and number of generations were taken to be  $N_p = 2000$  and  $N_g = 3000$ . It was observed that convergence was obtained in 1000 generations.

A plot of the Jiles–Atherton predicted loss and the FHM predicted loss (using the parameters obtained using the proposed fitting process) is shown in Fig. 4. As can be seen, the proposed model performed well in reproducing the error predicted by the Jiles–Atherton model for the training data set. The average error

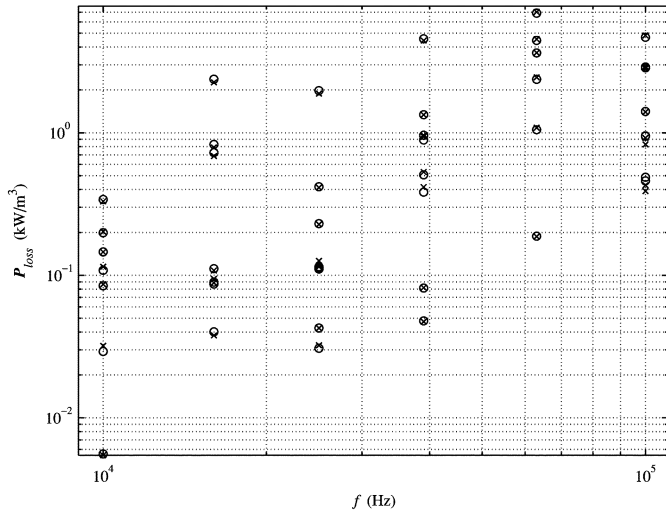


Fig. 4. Fit for FHM predicted loss (x) versus Jiles–Atherton predicted loss (o).

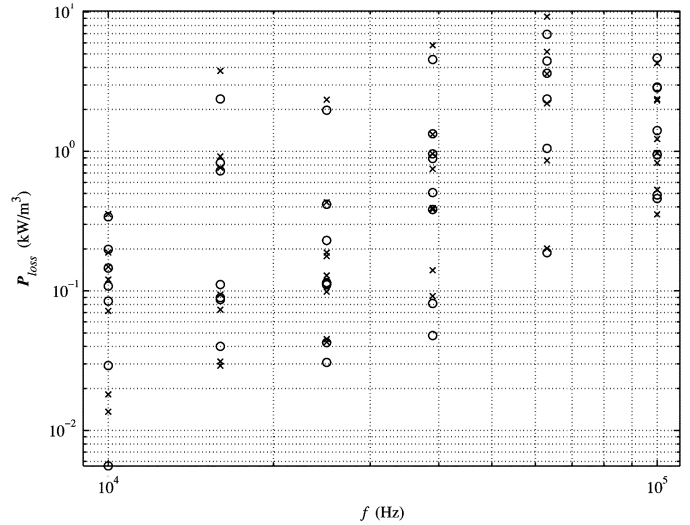


Fig. 5. Fit for MSE predicted loss (x) versus Jiles–Atherton predicted loss (o).

TABLE IV  
PARAMETERS OBTAINED FOR  $P_{FHM}$ : DC BIAS CASE

Parameter	Value	Parameter	Value
$m_1$	$1.86 \cdot 10^{-1}$	$s_1$ (J/Wb·m)	$5.14 \cdot 10^{-1}$
$m_2$	1.20	$s_2$ (J/Wb·m)	$1.81 \cdot 10^{-4}$
$b_1$	$8.45 \cdot 10^{-1}$	$r_1$	1.73

for the samples was 3.8%. This yielded the parameters shown in Table IV.

In order to compare the power losses predicted by the FHM and the MSE, the parameters  $C_1$  and  $C_2$  in (16) were determined by minimizing the average error between the predicted losses from the MSE and Jiles–Atherton model using curve-fitting (Nelder–Mead simplex [24]). The best fit parameters obtained were  $C_1 = 2.67$  and  $C_2 = 0.41$ .

A plot of the fitted and simulated power losses after the curve fitting process for the MSE is shown in Fig. 5. Each point corresponds to a separate experiment for different frequencies. The points at each frequency have different excitation waveforms. The average error for the samples was 24.7%, roughly an order of magnitude greater than the error associated with the FHM.

Ten sample waveforms having the form of (28), but different from the training waveforms were generated. The magnetic power losses associated with the ten sample waveforms using the FHM and MSE (with their fitted parameters) were then compared with the losses obtained from the Jiles–Atherton model. Table V lists the sample waveform data and the power losses. As shown at the bottom of Table V, the losses obtained from the FHM were comparable to the Jiles–Atherton model in the dc bias case. The FHM is also shown to yield considerably less error than the MSE.

At this point, it is interesting to observe the effect of each term in the FHM. In Fig. 6,  $\zeta(f)$  is plotted with respect to frequency. As shown in Fig. 6,  $\zeta(f)$  increases with increasing frequency. Note that this term is independent of the applied field. It can therefore be thought of as accounting for the frequency dependency of the coercivity of the material, which causes an expansion of the hysteresis loop for a given quasi-static field.

TABLE V  
COMPARISON OF CALCULATED POWER LOSS FROM TIME-DOMAIN ANALYSIS VERSUS MSE AND FHM

$H_{min}$ (A/m)	$H_{max}$ (A/m)	$f$ (kHz)	$P_{JA}$ (kW/m <sup>3</sup> )	$P_{MSE}$ (kW/m <sup>3</sup> )	$P_{FHM}$ (kW/m <sup>3</sup> )	
91.30	119.99	10	0.56	0.67	0.50	
132.22	166.61	20	0.93	1.45	0.94	
75.97	111.94	30	3.92	4.26	3.53	
64.26	107.03	40	10.29	9.62	8.83	
105.97	146.14	50	5.30	7.10	5.29	
117.45	146.11	60	2.42	2.99	2.53	
85.35	117.98	70	6.77	7.25	6.45	
123.65	147.22	80	2.12	1.99	2.04	
120.55	162.84	90	9.50	13.47	9.89	
51.71	87.16	100	25.28	19.15	20.60	
Avg. Error (%)				26.6	7.1	

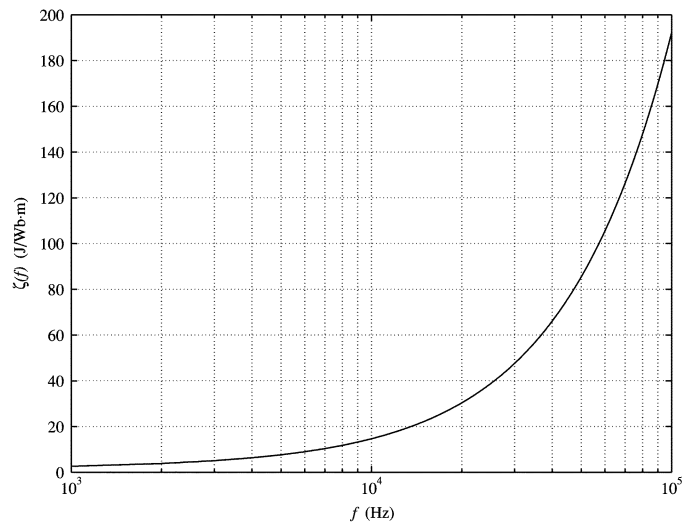


Fig. 6.  $\zeta(f)$  versus frequency.

In Figs. 7 and 8,  $z(\Delta M_{an})$  is plotted with respect to the dc field  $H_{dc} = (H_{max} - H_{min})/2$  and  $\Delta H$ . Fig. 8 depicts the level set of  $z(\Delta M_{an})$ . As shown in Figs. 7 and 8, for a given

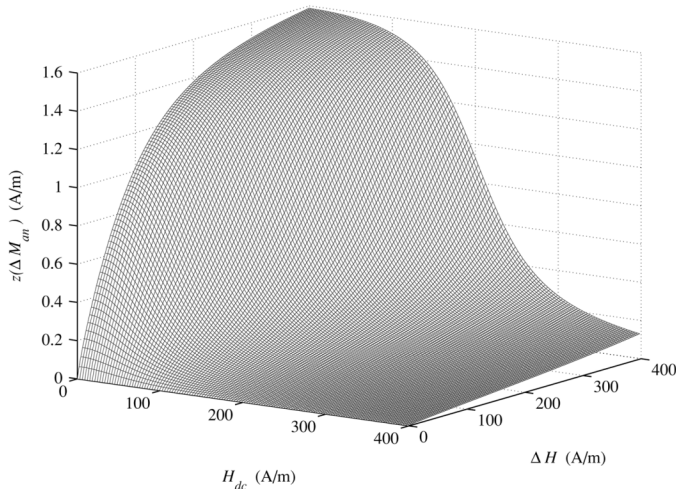


Fig. 7.  $z(\Delta M_{an})$  versus  $H_{dc}$  and  $\Delta H$ .

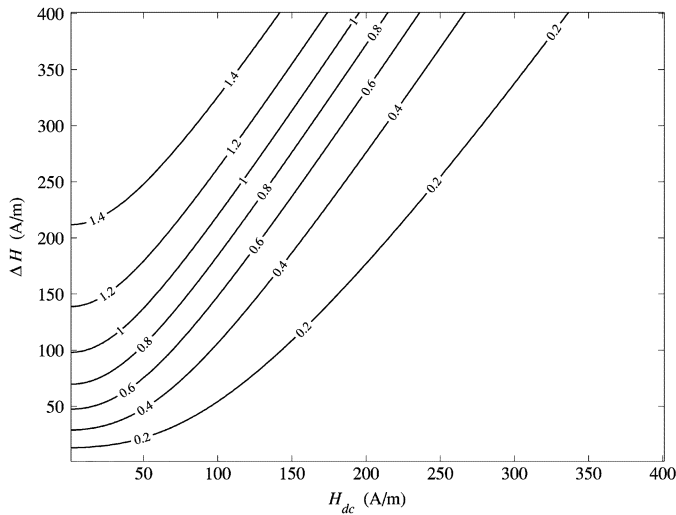


Fig. 8. Level set of  $z(\Delta M_{an})$ .

$\Delta H$ ,  $z(\Delta M_{an})$  decreases as the dc field reaches the saturation field (approximately 200 A/m for 3C81). For zero dc bias, the function is seen to have the form of the anhysteretic magnetization characteristic. This term accounts for loss attributable to the “height” of the  $B-H$  loop, while incorporating saturation of the magnetic material.

In Fig. 9,  $w(\Delta H)$  is plotted with respect to  $\Delta H$ . This term accounts for loss attributable to the “width” of the  $B-H$  loop.

V. CASE STUDY

In order to demonstrate the use of the proposed model in a practical problem, and at the same time provide additional validation on a data set independent of the data set used to characterize the model parameters, an EI core inductor is now considered. In particular, for a given EI core inductor the losses computed using the FHM, MSE, and Jiles–Atherton model will be compared at a number of operating points corresponding to different bias levels and fundamental frequencies.

In order to calculate the total inductor magnetic loss, it is necessary to compute the magnetic loss associated with the fields

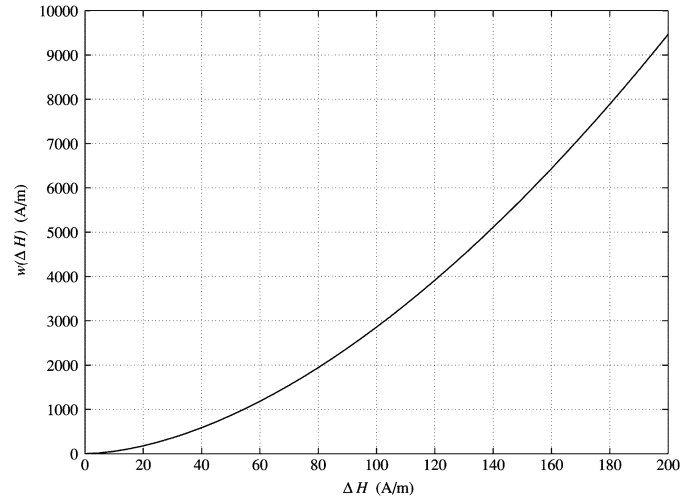


Fig. 9.  $w(\Delta H)$  versus  $\Delta H$ .

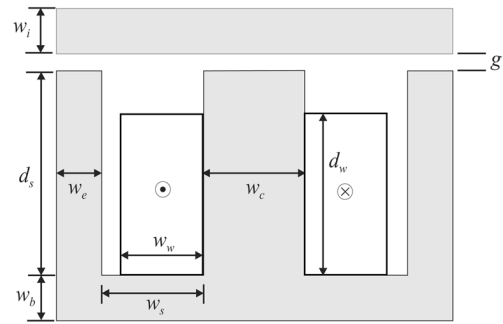


Fig. 10. An “EI” type ferrimagnetic inductor.

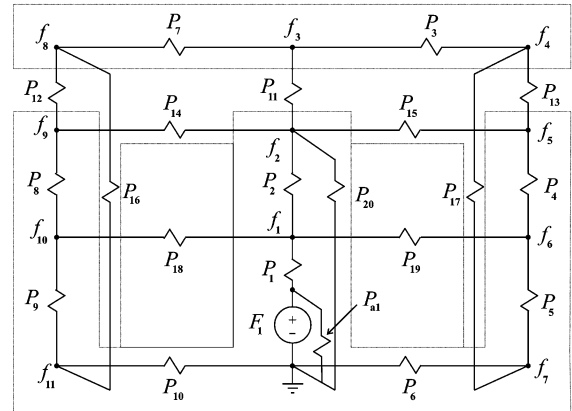


Fig. 11. HFMEC representation of the inductor in Fig. 10.

throughout the device for a given operating condition. In [12], an HFMEC representation of the EI type ferrimagnetic inductor was derived. The arrangement of the EI inductor is depicted in Fig. 10; its HFMEC representation is shown in Fig. 11. All symbols in Figs. 10 and 11 are defined in [12].

For this study, it will be assumed that the EI inductor in Fig. 10 is functioning as the filter inductor in a power electronic dc-dc (buck) converter.

In a buck converter, the desired (controlled) inductor currents are triangular with dc bias. For the FHM and MSE, the first

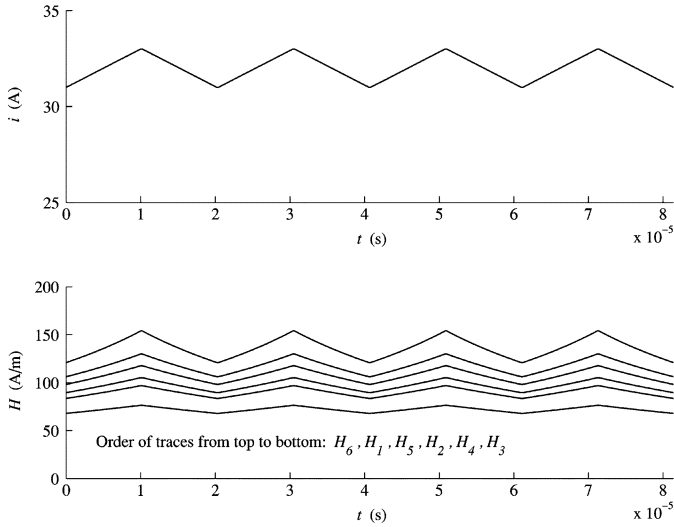


Fig. 12. Input current and fields in several segments of the HFMEC.

TABLE VI  
COMPARISON OF CALCULATED POWER LOSS FROM TIME-DOMAIN ANALYSIS  
VERSUS MSE AND FHM IN THE EI INDUCTOR

Seg.	$H_{min}$ (A/m)	$H_{max}$ (kHz)	$P_{JA}$ (kW/m <sup>3</sup> )	$P_{MSE}$ (kW/m <sup>3</sup> )	$P_{FHM}$ (kW/m <sup>3</sup> )
1	106.16	129.86	1.40	0.86	1.50
2	89.54	105.16	0.62	0.62	0.69
3	67.92	76.34	0.19	0.19	0.21
4	83.54	96.80	0.45	0.51	0.51
5	98.13	117.61	0.96	0.75	1.04
6	120.94	153.93	2.64	1.03	2.74
		Total Loss (W)	10.5	6.4	11.2
		Error (%)		38.6	6.7

step is to compute  $H_{min}$ ,  $H_{max}$  and  $B_{min}$ ,  $B_{max}$  in each element using the HFMEC. This is done based on the minimum and maximum input current,  $i_{min}$  and  $i_{max}$ , respectively. Then the FHM and MSE are used to predict the loss density in each segment, whereupon the losses are summed to compute the total loss as follows. In Fig. 11, the permeances of the magnetic core segments (as opposed to leakage permeances) are denoted  $P_j$ , where  $j \in \{1, 2, \dots, 10\}$ . Let the magnetic loss per unit volume in core segment  $j$  computed from model “X” be denoted  $P_{X,j}$ . Using symmetry, the total magnetic loss  $P_{total}$  in the inductor is

$$P_{total} = \sum_{j=1}^2 V_j P_{X,j} + 2 \sum_{j=3}^6 V_j P_{X,j} \quad (31)$$

where  $V_j$  is the volume of the  $j$ th segment, and the segment number matches the permeance subscript in Fig. 11.

For comparison purposes, the losses were also computed using the Jiles–Atherton model. The first step in this case was to generate the time history of the fields within the inductor using the HFMEC. These fields served as the input to the Jiles–Atherton model, from which the magnetizations in each segment were obtained. As an example, the bottom traces in Fig. 12 depict the fields for the input current waveform shown in the upper trace. In particular, the field intensity  $H_1$  through  $H_6$  correspond to the permeance element  $P_1$  through  $P_6$  in Fig. 11.

TABLE VII  
COMPARISON OF CALCULATED POWER LOSS FROM TIME-DOMAIN ANALYSIS  
VERSUS MSE AND FHM FOR  $D = 0.25$

$H_{min}$ (A/m)	$H_{max}$ (A/m)	$f$ (kHz)	$P_{JA}$ (kW/m <sup>3</sup> )	$P_{MSE}$ (kW/m <sup>3</sup> )	$P_{FHM}$ (kW/m <sup>3</sup> )
121.0	192.1	10	1.76	1.07	1.82
100.6	151.7	20	3.32	2.79	3.45
97.5	135.8	30	9.61	4.83	10.01
59.1	112.0	40	10.37	4.43	11.27
68.1	104.7	50	7.71	6.93	8.14
128.6	169.4	60	8.71	7.90	9.15
76.0	111.9	70	17.14	7.86	19.02
64.3	107.0	80	11.26	10.12	11.81
100.3	149.6	90	36.76	9.71	43.68
120.5	162.8	100	21.80	10.29	24.18
			Avg. Error (%)	37.2	7.6

TABLE VIII  
COMPARISON OF CALCULATED POWER LOSS FROM TIME-DOMAIN ANALYSIS  
VERSUS MSE AND FHM FOR  $D = 0.50$

$H_{min}$ (A/m)	$H_{max}$ (A/m)	$f$ (kHz)	$P_{JA}$ (kW/m <sup>3</sup> )	$P_{MSE}$ (kW/m <sup>3</sup> )	$P_{FHM}$ (kW/m <sup>3</sup> )
121.0	192.1	10	1.77	1.07	1.82
100.6	151.7	20	3.34	2.80	3.45
97.5	135.8	30	9.67	4.85	10.01
59.1	112.0	40	10.45	4.46	11.27
68.1	104.7	50	7.77	6.97	8.14
128.6	169.4	60	8.80	7.99	9.15
76.0	111.9	70	17.30	7.89	19.02
64.3	107.0	80	11.39	10.22	11.81
100.3	149.6	90	37.10	9.76	43.68
120.5	162.8	100	22.06	10.39	24.18
			Avg. Error (%)	37.3	7.6

TABLE IX  
COMPARISON OF CALCULATED POWER LOSS FROM TIME-DOMAIN ANALYSIS  
VERSUS MSE AND FHM FOR  $D = 0.75$

$H_{min}$ (A/m)	$H_{max}$ (A/m)	$f$ (kHz)	$P_{JA}$ (kW/m <sup>3</sup> )	$P_{MSE}$ (kW/m <sup>3</sup> )	$P_{FHM}$ (kW/m <sup>3</sup> )
121.0	192.1	10	1.77	1.07	1.82
100.6	151.7	20	3.34	2.80	3.45
97.5	135.8	30	9.67	4.85	10.01
59.1	112.0	40	10.45	4.45	11.27
68.1	104.7	50	7.76	6.97	8.14
128.6	169.4	60	8.77	7.98	9.15
76.0	111.9	70	17.28	7.90	19.02
64.3	107.0	80	11.35	10.19	11.81
100.3	149.6	90	37.09	9.75	43.68
120.5	162.8	100	22.00	10.37	24.18
			Avg. Error (%)	37.3	7.6

In Table VI, the minimum and maximum fields produced by the input current in Fig. 12 are listed for segments 1–6 of the inductor. Power losses from the Jiles–Atherton model, MSE, and FHM are also shown for each segment. The bottom of Table VI lists the total power calculated from (31) and the error with respect to the Jiles–Atherton model.

In the next study, the effect of current waveform duty cycle was investigated. To this end, ten sample minimum and maximum current points were generated. From these points, triangular waveforms of duty cycle  $D = 0.25$ ,  $D = 0.50$ , and

$D = 0.75$  were produced, yielding a total of 30 waveforms. The total magnetic power losses associated with the ten sample waveforms using the FHM and MSE were then compared with the losses obtained from the Jiles–Atherton model.

In this study, in order to ensure the least possible error using the MSE, the parameters  $k_1$  and  $k_2$  in (16) were obtained for each waveform. This was done by minimizing the average error in the predicted power losses between the Jiles–Atherton model and the MSE in segments 1–6 for each current waveform.

Tables VII–IX show the sample waveform data and the power losses for the different duty cycles. As shown at the bottom of Tables VII–IX, the losses obtained from the FHM were comparable to the Jiles–Atherton model and yielded considerably less error than the MSE, for all of the duty cycles.

## VI. CONCLUSION

In this work, a model and parameter identification procedure was demonstrated that yielded a closed-form, time-independent hysteresis loss equation from a sample of time-domain simulations. The accuracy of the power losses obtained from the new model was shown to be consistent with a frequency-dependent Jiles–Atherton simulation and yielded better performance than the MSE for sinusoidal zero dc bias and triangular waveforms with dc bias. The usefulness of the new model was demonstrated with a case study in which power loss arising from field waveforms in a power electronic filter inductor for various converter duty cycles were also shown to be consistent with the time-domain solution. The proposed model and characterization procedure is therefore a computationally efficient and accurate method of computing magnetic losses for high-frequency ferromagnetic component design.

## ACKNOWLEDGMENT

This work was supported in part by the Electric Ship Research and Development Consortium (ESRDC) and the Office of Naval Research under Grant N00014-02-1-0623.

## REFERENCES

- [1] A. Kerkoff and H. Ling, "Design of a band-notched planar monopole antenna using genetic algorithm optimization," *IEEE Trans. Antennas Propag.*, vol. 55, no. 3, pp. 604–610, Mar. 2007.
- [2] S. Cui, D. S. Weile, and J. L. Volakis, "Novel planar electromagnetic absorber designs using genetic algorithms," *IEEE Trans. Antennas Propag.*, vol. 54, no. 6, pp. 1811–1817, Jun. 2006.
- [3] L. Jolly, M. A. Jabbar, and L. Qinghua, "Design optimization of permanent magnet motors using response surface methodology and genetic algorithms," *IEEE Trans. Magn.*, vol. 41, no. 10, pp. 3928–3930, Oct. 2005.
- [4] Y. D. Chun, S. Wakao, T. H. Kim, K. B. Jang, and J. Lee, "Multiobjective design optimization of brushless permanent magnet motor using 3D equivalent magnetic circuit network method," *IEEE Trans. Appl. Supercond.*, vol. 14, no. 2, pp. 910–913, Jun. 2004.
- [5] N. Jin and Y. Rahmat-Samii, "Parallel particle swarm optimization and finite-difference time-domain (PSO/FDTD) algorithm for multiband and wide-band patch antenna designs," *IEEE Trans. Antennas Propag.*, vol. 53, no. 11, pp. 3459–3468, Nov. 2005.
- [6] S. L. Ho, S. Yang, G. Ni, E. W. C. Lo, and H. C. Wong, "A particle swarm optimization-based method for multiobjective design optimizations," *IEEE Trans. Magn.*, vol. 41, no. 5, pp. 1756–1759, May 2005.
- [7] C. P. Steinmetz, "On the law of hysteresis," *Proc. IEEE*, vol. 72, no. 2, pp. 196–221, Feb. 1994.
- [8] J. Reinert, A. Brockmeyer, and R. W. A. A. De Doncker, "Calculation of losses in ferro- and ferrimagnetic materials based on the modified Steinmetz equation," *IEEE Trans. Ind. Appl.*, vol. 37, no. 4, pp. 1055–1061, Jul. 2001.
- [9] A. Van den Bossche, V. C. Valchev, and G. B. Georgiev, "Measurement and loss model of ferrites with non-sinusoidal waveforms," in *Power Electron. Specialists Conf.*, Jul.–Aug. 2001, vol. 6, pp. 4814–4818.
- [10] L. Jieli, T. Abdallah, and C. R. Sullivan, "Improved calculation of core loss with nonsinusoidal waveforms," in *Power Electron. Specialists Conf.*, Sep. 30–Oct. 4, 2001, vol. 4, pp. 2203–2210.
- [11] K. Venkatachalam, C. R. Sullivan, T. Abdallah, and H. Tacca, "Accurate prediction of ferrite core loss with nonsinusoidal waveforms using only Steinmetz parameters," in *COMPEL 2002. IEEE Workshop Comput. Power Electronics. Proc.*, Mayaguez, Puerto Rico, Jun. 3–4, 2002, pp. 36–41.
- [12] J. Cale, S. D. Sudhoff, and L. Q. Tan, "Accurately modeling EI core inductors using a high-fidelity magnetic equivalent circuit approach," *IEEE Trans. Magn.*, vol. 42, no. 1, pp. 40–46, Jan. 2006.
- [13] D. Jiles, *Introduction to Magnetic Materials*, 2nd ed. London, U.K.: Chapman & Hall, 1998.
- [14] D. C. Jiles, "A self consistent generalized model for the calculation of minor loop excursions in the theory of hysteresis," *IEEE Trans. Magn.*, vol. 28, no. 5, pp. 2602–2604, Sep. 1992.
- [15] D. C. Jiles, "Frequency dependence of hysteresis curves in 'non-conducting' magnetic materials," *IEEE Trans. Magn.*, vol. 29, no. 6, pp. 3490–3492, Nov. 1993.
- [16] R. Ridley, "Modeling ferrite core losses," *Switching Power Mag.*, vol. 3, no. 1, pp. 6–13, 2002.
- [17] D. E. Goldberg, *Genetic Algorithms in Search, Optimization, and Machine Learning*. Boston, MA: Addison-Wesley, 2001.
- [18] K. Deb, *Multi-Objective Optimization Using Evolutionary Algorithms*. New York: Wiley, 2001.
- [19] E. K. P. Chong and S. H. Zak, *An Introduction to Optimization*, 2nd ed. New York: Wiley, 2001.
- [20] Ferroxcube Material Specifications: Ferrites for Power Applications pp. 87–90 [Online]. Available: <http://www.ferroxcube.com>
- [21] "Math Works, Matlab," The Math Works. Natick, MA, 1994.
- [22] K. Sayood, *Learning Programming Using MATLAB*. San Rafael, CA: Morgan & Claypool, 2007.
- [23] Energy Systems Analysis Consortium (ESAC) Genetic Optimization Based System Engineering Tool (GOSET). ver. 2.01, School of Elect. Comput. Eng., Purdue Univ., West Lafayette, IN, 2003.
- [24] J. A. Nelder and R. Mead, "A simplex method for function minimization," *Comput. J.*, vol. 7, pp. 308–313, 1965.

Manuscript received July 26, 2007; revised March 18, 2008. Corresponding author: R. R. Chan (e-mail: riyadi@purdue.edu).

**J. Cale** (M'03) received the B.S. (*summa cum laude*) degree in electrical engineering from the University of Missouri-Rolla in 2001, and M.S. and Ph.D. degrees in electrical engineering from Purdue University, West Lafayette, IN., in 2003 and 2007, respectively.

He served in the United States Army Reserves from 1994–2003 and interned at the Cooper Nuclear Reactor in Brownville, NE in 2000. His interests include electric machinery and drives, power electronics, electromagnetics, and genetic algorithms.

**S. D. Sudhoff** (SM'01) received the B.S. (highest distinction), M.S., and Ph.D. degrees from Purdue University, West Lafayette, IN, in 1988, 1989, and 1991, respectively.

He served as Visiting Faculty with Purdue University from 1991 to 1993. He was also a Faculty Member at the University of Missouri-Rolla from 1993 to 1997, and he joined the faculty of Purdue University in 1997. His interests include electric machines, power electronics, finite-inertia power systems, applied control, and genetic algorithms. He has published over 50 journal papers in these areas, including six prize papers.

**R. R. Chan** (M'05) received the B.S. and M.S. degrees in electrical engineering from Purdue University, West Lafayette, IN, in 2003 and 2005, respectively. He is currently working towards the Ph.D. degree in electrical engineering at Purdue University.

His research interest include power electronics, power systems, and population-based optimization techniques.